Frequency Domain Spectroscopy in Rare-Earth-Doped Gain Media

Emir Salih Magden, Patrick Callahan, Nanxi Li, Jonathan D. B. Bradley, Neetesh Singh, Alfonso Ruocco, Leslie A. Kolodziejski, Erich P. Ippen, and Michael R. Watts

***Abstract*—Many spectroscopic techniques today rely on time-resolved measurements under short excitation pulses. Instead of using a chopped pump excitation, or ultrafast optical pulses, we expand on and apply the previously developed set of frequency domain methods to analyze the population level dynamics in rare-earth-doped media. By identifying the full frequency response of the gain medium, this method can accurately yield excited state lifetimes and can also be used to estimate transition cross-sections. The accuracy of the frequency domain methods are verified with Er^{3+}- and Tm^{3+}-doped fibers, and an $Al_2O_3:Tm^{3+}$ waveguide, recovering similar results as reported by time-resolved techniques. The complete frequency domain model presented here can be used in characterization of novel optical gain media, and can provide insights into population dynamics in solid state amplifiers and lasers.**

***Index Terms*—Rare-earth metals, optical pumping, laser amplifiers, frequency domain analysis.**

I. Introduction

SPECTROSCOPIC parameters such as lifetimes and transition cross-sections are essential pieces of information for understanding population level dynamics in gain media. Many optical phenomena including absorption, laser emission, saturation, and even high-order effects like energy transfer upconversion and cross-relaxation can be modeled by using excited state lifetimes and transition rates between energy states [1]–[5]. Knowledge of these spectroscopic properties is therefore essential for understanding the photon dynamics in amplifiers and lasers.

With the development of novel photonic materials engineered for enhanced spectroscopic properties [6]–[9], measurements of transition cross-sections and excited state lifetimes are becoming important problems of topical interest. A wide range of materials have been studied for their fluorescence and excited state lifetimes after Gaviola's demonstration of what he called the fluorometer in 1927 [10]. In general, most lifetime measurements are performed using either time-resolved or frequency domain techniques [11]. For time domain measurements, in order to resolve the transient response, pump excitations that can be modulated with rise/fall times much shorter than the lifetime are typically required [12]. Earlier time domain measurements were based on pumping the active medium with a pulsed excitation created either by flash lamps [13]–[15], or by mechanically chopped continuous-wave pump lasers [16], [17]. Later on, many doped crystals [18], [19], fibers [20], [21], and waveguides [22]–[24] have been characterized for their excited state lifetimes using mechanical choppers. Depending on the required pump duration and the media studied, the excitation signal can also be modulated with a pulsed electrical pump [25]; or an external electro-optic [26], [27] or acousto-optic modulator [28], [29] may be used. It is also possible to use pulsed sources such as Q-switched [30], or mode-locked femtosecond lasers [31] to create the required pulsed excitations. Another time domain technique involves the use of step-scan Fourier transform infrared (FTIR) spectroscopy to study time-resolved absorbance. In contrast to a wavelength-by-wavelength measurement, an FTIR spectroscope gives access to the whole infrared region in one measurement by using a broadband infrared source and a Michelson interferometer with a movable mirror [32]. Time domain data is collected from the change in absorbance of the studied sample, resulting in spectral data as a function of time and wavelength [33], [34]. For all time-resolved measurements, the recorded time domain data is analyzed for exponential decay components, where one or multiple time-constants [35] or a continuous lifetime distribution [36]–[38] can be extracted depending on the number and types of luminescent species studied.

The fluorescence can also be analyzed in the frequency domain, where the sample is excited with a pump whose intensity is sinusoidally modulated. The lifetime of the excited sample results in a phase shift between the intensity-modulated pump and the resulting fluorescence [39]–[41]. Moreover, the modulation amplitude of fluorescence is gradually attenuated

Manuscript received November 30, 2017; revised February 4, 2018; accepted February 6, 2018. Date of publication February 13, 2018; date of current version March 28, 2018. This work was supported under the DARPA DODOS project, Contract HR0011-15-C-0056. *(Corresponding author: Emir Salih Magden.)*

E. S. Magden is with Koç University, Istanbul 34350, Turkey, and also with the Research Laboratory of Electronics, Massachusetts Institute of Technology, Cambridge, MA 02139 USA (e-mail: esmagden@ku.edu.tr).

N. Li is with Harvard University, Cambridge, MA 02138 USA, and also with the Research Laboratory of Electronics, Massachusetts Institute of Technology, Cambridge, MA 02139 USA (e-mail: nanxili@g.harvard.edu).

J. D. B. Bradley is with McMaster University, Hamilton, ON L8S 4L8 Canada, and also with the Research Laboratory of Electronics, Massachusetts Institute of Technology, Cambridge, MA 02139 USA (e-mail: jbradley@mcmaster.ca).

A. Ruocco is with Cambridge University, Cambridge CB2 1TN, U.K., and also with the Research Laboratory of Electronics, Massachusetts Institute of Technology, Cambridge, MA 02139 USA (e-mail: aruocco@mit.edu).

P. Callahan, N. Singh, L. A. Kolodziejski, E. P. Ippen, and M. R. Watts are with the Research Laboratory of Electronics, Massachusetts Institute of Technology, Cambridge, MA 02139 USA (e-mail: pcallahn@mit.edu; neeteshs@mit.edu; leskolo@mit.edu; ippen@mit.edu; mwatts@mit.edu).

Color versions of one or more of the figures in this paper are available online at http://ieeexplore.ieee.org.

Digital Object Identifier 10.1109/JSTQE.2018.2805807

with increasing driving frequency, due to the finite system bandwidth. Measurements taking advantage of this phase shift and the corresponding attenuation have been demonstrated in the past [42]–[46]. Many biochemical samples have been studied using these frequency domain techniques [47]–[50], resolving lifetimes as short as a picosecond. However, despite its versatility, the general family of frequency domain spectroscopic techniques has not been widely used in the characterization of solid state gain media. Specifically, no analyses of pump and signal power dependence of the frequency response, or applications to measurements other than the lifetime have been found.

In this paper, we study the above described frequency domain analysis in detail by deriving the complete transfer function between a modulated pump input and the signal output in rare-earth doped glass media. We analyze the dependence of system behavior on signal and pump rates in the frequency domain, and confirm the transfer function approximation by numerical simulations of the rate equations. We then use this system description for accurately measuring the spontaneous emission lifetime and pump absorption cross-sections in rare-earth doped gain media. After verifying our methods in Er^{3+}- and Tm^{3+}-doped fibers, we characterize thulium-doped aluminum oxide ($\mathrm{Al_2O_3}$:Tm^{3+}) waveguides. These newly found parameters can be utilized to design high performance amplifiers and lasers in the $1.8\ \mu\mathrm{m} - 1.9\ \mu\mathrm{m}$ gain spectrum of Tm^{3+} [51], [52].

II. Two-Level Population Model with an Amplitude-Modulated Pump

To model a sinusoidally modulated excitation in rare-earth doped media, we represent the gain medium with a two-level system. The use of a two-level system is validated by the following assumptions: The steady state pump power is low, there are already only a few energy levels accessible due to pump photons being low enough in energy, and some higher energy states rapidly decay to the upper lasing level [3]. For systems pumped stronger with higher-energy photons or those with longer-lived higher-energy states, a general frequency domain analysis is presented in the appendix.

The populations of the two levels are governed by the rate equations that describe the rate of change of the number of rare-earth ions in the ground or excited states. Here, we will refer to the total population by N_t, the population in the ground state by N_0, and the population in the excited state by N_1, where $N_0 + N_1 = N_t$ at all times. As N_t is constant, the rates of change in N_0 and N_1 have the same magnitude with opposite signs. This rate of change is dictated by stimulated signal and pump absorption from the ground state, and the stimulated and spontaneous signal emission from the excited state as described by

$$\frac{dN_0}{dt} = -\frac{dN_1}{dt} = \underbrace{-\sigma_{\mathrm{sa}}\phi_s N_0 - \sigma_{\mathrm{pa}}\phi_p(1+m(t))N_0}_{\text{stimulated signal and pump absorption}} + \underbrace{\sigma_{\mathrm{se}}\phi_s N_1}_{\substack{\text{stimulated}\\ \text{emission}}} + \underbrace{\frac{N_1}{\tau}}_{\substack{\text{spontaneous}\\ \text{emission}}} \tag{1}$$

where ϕ_p and ϕ_s are the rates of pump and signal photons per unit area, σ_{pa}, σ_{sa}, and σ_{se} are the signal absorption, pump absorption, and signal emission cross-sections, and τ is the spontaneous emission lifetime. Pump and signal rates can be expressed as $\phi_{p,s} = I_{p,s}/(h\nu_{p,s})$ where h is Planck's constant, $I_{p,s}$ are the intensities, and $\nu_{p,s}$ are the frequencies of the pump and signal photons respectively. Here, we have added a modulation term $m(t)$ to represent the introduced perturbation to the otherwise constant pump rate. In (1), we can separate the modulation dependent pump absorption, and rewrite the rate of change of the ground state population as

$$\frac{dN_0}{dt} = -\frac{N_0}{\tau_{\mathrm{eff}}} + N_t\left(\sigma_{\mathrm{se}}\phi_s + \frac{1}{\tau}\right) - \sigma_{\mathrm{pa}}\phi_p N_0 m(t) \tag{2}$$

where we defined the effective lifetime

$$\frac{1}{\tau_{\mathrm{eff}}} = (\sigma_{\mathrm{sa}} + \sigma_{\mathrm{se}})\,\phi_s + \sigma_{\mathrm{pa}}\phi_p + \frac{1}{\tau} \approx \sigma_{\mathrm{pa}}\phi_p + \frac{1}{\tau} \tag{3}$$

for $\phi_s \ll \phi_p$. Here, choosing to operate with a signal rate much smaller than the pump rate allows us to simplify the effective lifetime. This yields $1/\tau_{\mathrm{eff}}$ as a linear function of ϕ_p, with a proportionality constant of σ_{pa} and a vertical intercept of $1/\tau$. From the description in (3), σ_{pa} and $1/\tau$ can be independently determined from a dataset of $(\phi_p, 1/\tau_{\mathrm{eff}})$ pairs. Moreover, even if the exact pump rate ϕ_p cannot be characterized due to various pump coupling losses, as long as the pump power from the source is well known, the vertical intercept $1/\tau$ can still be precisely calculated.

So far, we assumed that all the pump power input into the system goes into modulating the population levels where the signal mode spatially exists. Although this is a good approximation for fibers, many waveguides in the tight confinement regime have non-perfectly overlapping pump and signal modes due to strong waveguide dispersion. We must therefore let $\phi_p = \phi_{p0}\Gamma$ where ϕ_{p0} is the original input pump rate, and define the pump-signal intensity overlap factor by

$$\Gamma = \frac{\iint_G e_p^* e_p e_s^* e_s\, da}{\left(\iint_\infty (e_p^* e_p)^2\, da \iint_\infty (e_s^* e_s)^2\, da\right)^{1/2}} \tag{4}$$

where e_p and e_s are the electric fields at the pump and signal wavelengths. The overlap integral in the numerator is calculated over the doped gain medium represented by region G, whereas the normalization integrals in the denominator are calculated over the whole waveguide cross-section.

In order to decouple the modulation dependence from the nominal population levels, we let $N_0 = N_{0(\mathrm{ss})} + \Delta N_0$, where $N_{0(\mathrm{ss})}$ is the steady state population in the ground state, and ΔN_0 is the change introduced due to the pump modulation. $N_{0(\mathrm{ss})}$ can be calculated from (2) by setting $m(t) = 0$, and is given by $N_{0(\mathrm{ss})} = N_t\tau_{\mathrm{eff}}(\sigma_{\mathrm{se}}\phi_s + 1/\tau)$. Equation (1) can then be written in terms of $N_{0(\mathrm{ss})}$ and ΔN_0, and is simplified to

$$\begin{aligned}\frac{d}{dt}\Delta N_0 &= -\frac{\Delta N_0}{\tau_{\mathrm{eff}}} - \sigma_{pa}\phi_p\left(N_{0(\mathrm{ss})} + \Delta N_0\right)m(t)\\ &\approx -\frac{\Delta N_0}{\tau_{\mathrm{eff}}} - \sigma_{\mathrm{pa}}\phi_p N_{0(\mathrm{ss})} m(t).\end{aligned} \tag{5}$$

Here, by restricting operation to only small modulation depths where $|m(t)| \ll 1$, we made sure that $\Delta N_0 \ll N_{0(\mathrm{ss})}$, and obtained a simple relationship between ΔN_0 and $m(t)$. The frequency dependence of ΔN_0 on $m(t)$ can be obtained from the Laplace transform of (5), yielding the single-pole transfer function

$$H_1(s) = \frac{\Delta N_0(s)}{M(s)} = -\frac{\sigma_{\mathrm{pa}}\phi_p N_{0(\mathrm{ss})}\tau_{\mathrm{eff}}}{1+s\tau_{\mathrm{eff}}} \tag{6}$$

where $\Delta N_0(s)$ and $M(s)$ are Laplace transforms of ΔN_0 and $m(t)$ respectively. Equation (6) describes a single-pole low-pass filter with corner frequency $s_0 = 1/\tau_{\mathrm{eff}}$. Physically, the low-pass response of $H_1(s)$ indicates that the population levels will lag behind the modulation $m(t)$; and the system will respond to the modulation with a bandwidth determined by the effective lifetime τ_{eff}.

Although the modulation dependence of population levels is predicted by (6), the experimentally observable quantities in a gain medium are typically the output pump and signal powers as measured by a photodetector. We therefore have to relate the population levels to the resultant optical output power at the pump or signal wavelengths. For the signal, the output power can be expressed by the input power modulated by the absorption and emission due to the changing population levels in the gain medium of length L, and is given by

$$\begin{aligned} P_{\mathrm{out}} &= P_{\mathrm{in}} \exp\left(-\sigma_{sa} N_0 L + \sigma_{\mathrm{se}} N_1 L\right) \\ &= P_{\mathrm{out(ss)}} \exp\left(-\left(\sigma_{\mathrm{sa}} + \sigma_{\mathrm{se}}\right)\Delta N_0 L\right) \end{aligned} \tag{7}$$

where we separated the signal output into its steady state level $P_{\mathrm{out(ss)}}$ and a time-varying exponential. Using $N_1 = N_t - N_0$ and the definition of $N_{0(\mathrm{ss})}$ above, it can be shown that $P_{\mathrm{out(ss)}} = P_{\mathrm{in}} \exp\left(\left(\sigma_{\mathrm{se}} N_t - \left(\sigma_{\mathrm{sa}} + \sigma_{\mathrm{se}}\right) N_{0(\mathrm{ss})}\right) L\right)$. Since ΔN_0 is small compared to $N_{0(\mathrm{ss})}$, (7) can be further simplified by a Taylor expansion of the exponential term, yielding

$$P_{\mathrm{out}} \approx P_{\mathrm{out(ss)}} \left(1 - \left(\sigma_{\mathrm{sa}} + \sigma_{\mathrm{se}}\right)\Delta N_0 L\right). \tag{8}$$

With this approximation, we can completely separate the signal output into its steady state and time-varying components by $P_{\mathrm{out}} = P_{\mathrm{out(ss)}} + \Delta P_{\mathrm{out}}$ where $\Delta P_{\mathrm{out}} = -P_{\mathrm{out(ss)}} \left(\sigma_{\mathrm{sa}} + \sigma_{\mathrm{se}}\right)\Delta N_0 L$.

Clearly, the change in the output power depends linearly on the population level change; and their transfer function includes no frequency dependence:

$$H_2(s) = \frac{\Delta P_{\mathrm{out}}(s)}{\Delta N_0(s)} = -P_{\mathrm{out(ss)}} \left(\sigma_{\mathrm{sa}} + \sigma_{\mathrm{se}}\right) L. \tag{9}$$

Therefore, the only phase shift between the modulation input $m(t)$ and the recorded change in the signal output power ΔP_{out} is due to $H_1(s)$. The overall transfer function is then calculated as

$$\begin{aligned} H(s) &= \frac{\Delta P_{\mathrm{out}}(s)}{M(s)} = H_1(s) H_2(s) \\ &= \frac{\sigma_{\mathrm{pa}}\phi_p N_{0(\mathrm{ss})}\tau_{\mathrm{eff}} P_{\mathrm{out(ss)}} \left(\sigma_{\mathrm{sa}} + \sigma_{\mathrm{se}}\right) L}{1+s\tau_{\mathrm{eff}}}. \end{aligned} \tag{10}$$

According to the low-pass frequency dependence indicated in (10), the signal output power will lag behind the pump modulation by an amount determined by the effective lifetime τ_{eff}. For modulations slower than τ_{eff}, the signal tracks the modulation closely, since the system is able to effectively respond to changes within its bandwidth. For modulations with time scales quicker than τ_{eff}, the system will attenuate the change in the signal output power, due to the low-pass filter response.

For systems with large $N_t L$ products, the decay of pump power along the propagation direction may be significant. Since the effective lifetime is pump power dependent, one would then expect different lifetimes at the beginning and at the end of the fiber or waveguide being tested. In that case, it may be necessary to solve (1) with a spatial discretization where the pump power can be treated as a piecewise constant function of length. In the following numerical simulations and experimental measurements, we made sure that the total absorption of pump power stays within a few dB so that no further spatial discretization is necessary.

III. Numerical Simulations of Signal Output Waveform

In order to validate the approximations we made in the derivation of the low-pass response model in (10), we investigate numerical solutions to (1) using various pump modulation parameters. For these numerical solutions, we assumed typical spectroscopic parameters from rare-earth doped glasses where $N_t = 10^{20}$ cm^{-3}, $\sigma_{\mathrm{pa,sa,se}} \approx 10^{-21}$ cm^2, and $\tau = 500$ μs in a 10 cm long fiber with mode diameter of 5 μm. Unless indicated otherwise by the variables in each numerical simulation, a pump modulation frequency of $f_0 = 2$ kHz, a signal input power of $P_{\mathrm{in}} = 10$ μW, and a steady-state pump power of 300 mW were used, yielding $2\pi f_0 \tau_{\mathrm{eff}} \approx 0.5$.

First, we characterize the system response as a function of the modulation amplitude m_0 using a sinusoidal pump modulation of the form $m(t) = m_0 \sin(2\pi f_0 t)$. In Fig. 1(a), we plot the normalized signal output in arbitrary units for $0.1 < m_0 < 0.9$. With increasing m_0, the signal output deviates from the sinusoidal response predicted by the linear system model in (10). For instance when $m_0 = 0.9$, the output signal tends to quickly saturate before the end of the first half-cycle of the pump modulation, due to the large initial increase in the pump rate. This large pump power also results in the near-complete population depletion of the ground state, saturating the amplifier and flattening the otherwise sinusoidal output signal level. In contrast, for small m_0, the output signal remains sinusoidal and can be modeled with the transfer function approximation above. Consequently, we set $m_0 = 0.1$ for all subsequent simulations and measurements.

Next, we study the effects of the pump modulation frequency on the resultant signal. In Fig. 1(b), we plot the signal output waveform with pump modulation frequencies from 50 Hz to 20 kHz with a nominal pump power of 300 mW. For each modulation frequency, the variation in the signal output ΔP_{out} is normalized to its own steady state value of $P_{\mathrm{out(ss)}}$. The dashed line indicates the expected 3 dB system bandwidth of $f = 1/(2\pi\tau_{\mathrm{eff}})$ where τ_{eff} is calculated with the spectroscopic parameters above. For modulations slower than the system bandwidth, the signal output stays in phase with the modulation

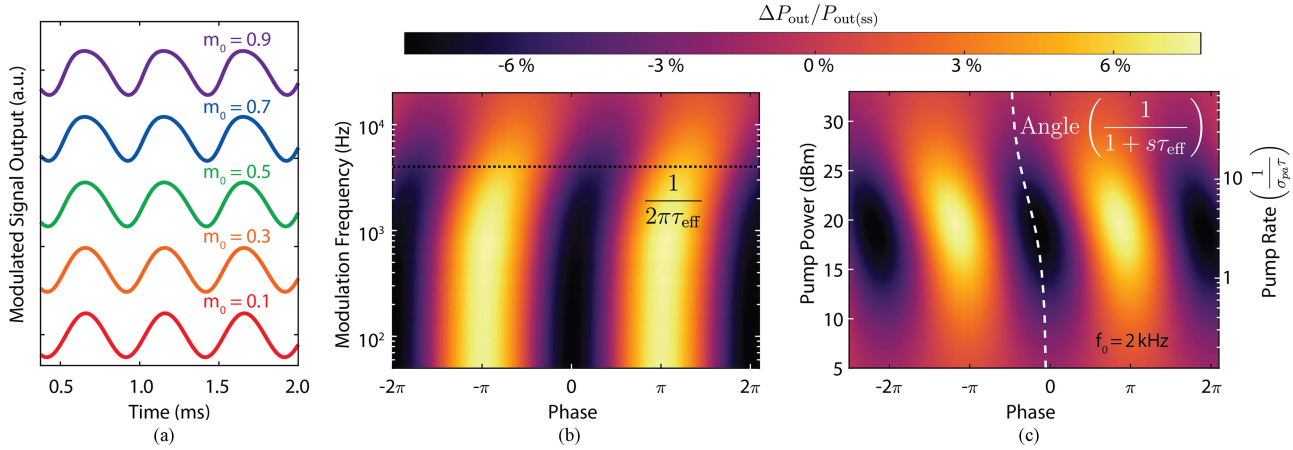

Fig. 1. Numerical simulations of signal output waveform as a function of (a) modulation depth m_0, (b) modulation frequency f_0, and (c) steady state pump rate ϕ_p. Waveforms plotted in (b) and (c) share the colorbar indicating the change in the signal output power with respect to the signal output with the unmodulated pump.

input. On the other hand, with faster modulations, the signal output lags behind the pump input as indicated by the tilting phase of the colored waveform. On the dashed line, the phase shift is exactly $\pi/4$ where the modulation frequency is equal to the system bandwidth. The numerical solutions also verify the predicted attenuation of the output signal for modulations above the 3 dB filter cutoff. This is indicated by the dropping contrast of the plotted waveform with increasing modulation frequency.

Finally in Fig. 1(c), we analyze the pump power dependence of the signal output waveform. As before, for each pump power simulated, ΔP_{out} is normalized to its own steady state value of $P_{\text{out(ss)}}$. Equivalent pump rates are plotted in the secondary vertical axis in corresponding spectroscopic units from (3). According to the numerical solutions, for pump powers less than 14 dBm ($\phi_p \sigma_{pa} \tau < 1$), the ground state stays mostly filled, and no significant change is expected in the signal output as absorption is only weakly modulated. For pump powers over 24 dBm ($\phi_p \sigma_{pa} \tau > 10$), gain is saturated due to the mostly-filled excited state; and the output signal power again does not exhibit significant change with respect to its steady state value. In contrast, when $1 < \phi_p \sigma_{\text{pa}} \tau < 10$, changes in pump power result in large variations in the signal phase shift. This variation is induced by τ_{eff}'s dependence on the pump rate ϕ_p, and is indicated by the tilts in the plotted signal waveforms. A higher pump rate results in a shorter effective lifetime; and the system exhibits a smaller phase shift due to reduced $2\pi\tau_{\text{eff}}$ product. Here, the dashed line indicates the expected phase shift from the transfer function in (10), and is equal to the angle of the complex quantity $1/(1 + s\tau_{\text{eff}})$. The excellent agreement of this dashed line with the tilted signal waveforms once again proves the validity of the approximations in the above derivation.

IV. Experimental Characterization of Rare-Earth-Doped Gain Media

We can utilize the change in the phase shift of the output signal to study system dynamics for various gain media. Specifically, due to the pump rate dependence of the effective lifetime, power dependent system response can be analyzed in order to accurately characterize spectroscopic parameters such as absorption and emission cross-sections, and the spontaneous emission lifetime. The experimental setup is shown in Fig. 2, where a rare-earth doped fiber or waveguide is pumped with a modulated pump laser. The signal is coupled to the gain medium with the use of a fiber wavelength division multiplexer. Modulated signal output is measured with a photodetector, and its amplitude and phase are compared to the modulation input using a lock-in amplifier. The advantages of frequency domain measurements for these materials are that only kHz modulation frequencies are required, and high signal-to-noise ratio is achieved by amplitude and phase measurements with lock-in amplifier averaging. For an accurate analysis by the lock-in amplifier, it is important to strongly attenuate any residual pump light at the detector. Even though typical InGaAs detectors usually have reduced responsivity at the shorter pump wavelengths for many rare-earth ions (976 nm for Er^{3+}, 785 nm for Tm^{3+}), we added a Si window for a stronger pump attenuation. The use of counter-propagating pump and signal lights can also provide additional extinction of the pump at the detector if necessary.

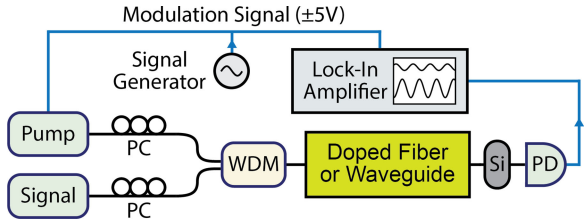

Fig. 2. Experimental setup for measuring the full transfer function of a rare-earth doped fiber or waveguide. PCs only used for the waveguide that requires transverse-electric pump and signal inputs. (PC: polarization controller, WDM: wavelength division multiplexer, PD: photodetector).

The key to accurate spectral characterization is identification of the effective lifetime τ_{eff} as a function of pump power as per (3). We first verify this method with two gain media that are well documented in literature: Er^{3+}-doped silica fiber, and Tm^{3+}-doped silica fiber. With the use of the lock-in amplifier, we measure the magnitude and phase of the transfer function between the change in the signal output and the pump modulation as a function of pump power. The magnitude and phase

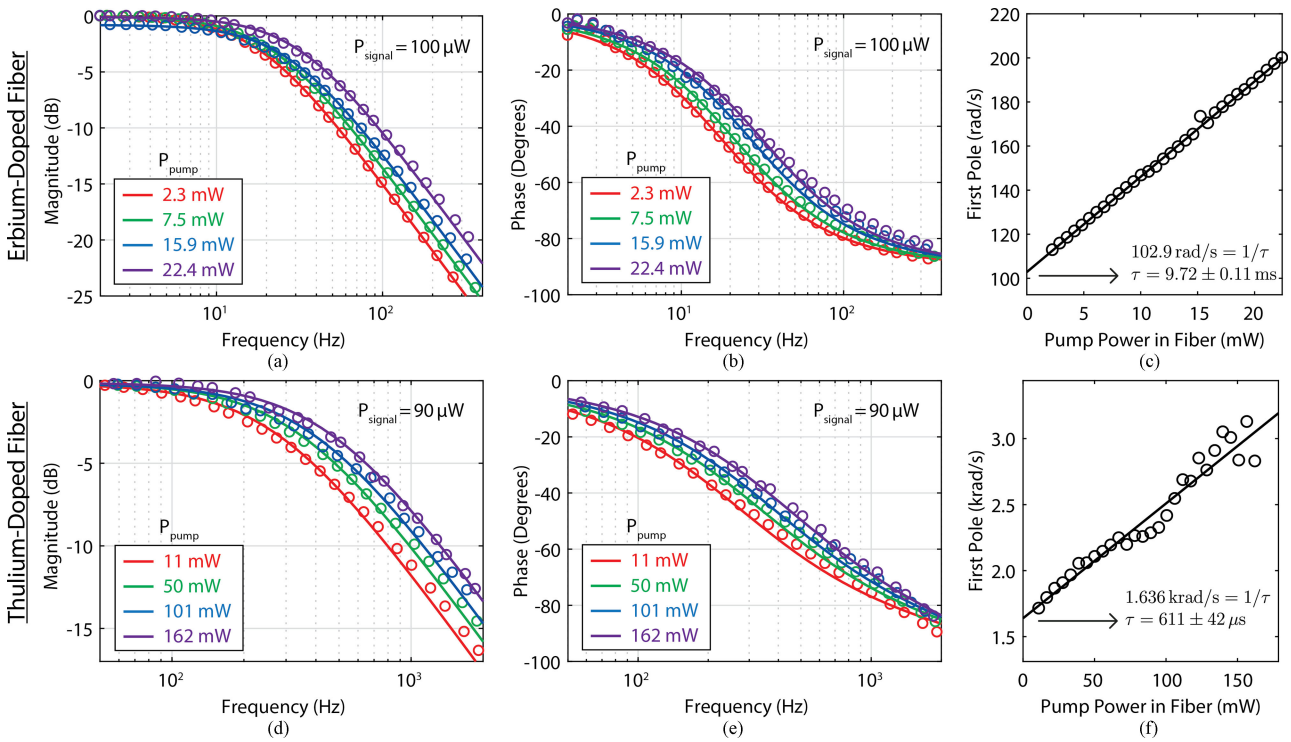

Fig. 3. (a)–(b) and (d)–(e) Magnitudes and phases of transfer functions for Er^{3+}-doped and Tm^{3+}-doped silica fibers measured with an amplitude-modulated continuous-wave pump. Linear fits to the first pole locations in (c) Er^{3+}-doped fiber and (f) Tm^{3+}-doped fiber.

responses for a single-mode, 10 cm long Er-doped fiber with 0.30 dB/cm peak absorption are plotted in Figs. 3(a) and (b). The 1550 nm signal power in the fiber was approximately 100 μW, much smaller than the 976 nm pump power which was over 1.5 mW. A least-squares fit was applied for each pump power to obtain the solid lines corresponding to the analytical transfer functions expected according to the model above. Both the magnitude and phase responses show excellent agreement with the single-pole filter description. Moreover, with increasing pump rate, the filter cutoff $1/(2\pi\tau_{\text{eff}})$ shifted to higher frequencies due to the reduced effective lifetime.

With a two-pole filter fit, to account for the possibility of a second lifetime, a second pole was found at a much higher frequency, indicating fast relaxations from higher energy states. However, the frequency of the first pole remained unchanged when compared with the single-pole transfer function fits. Even when the data were fit using the expected transfer function for a three-level system with two poles and a zero (see appendix), the location of the first pole did not change. In Fig. 3(c), we plot the location of this first pole as a function of pump power in the fiber. The data are accurately represented by the linear fit (solid line), in agreement with the linear pump power dependence in our definition of the effective lifetime. The vertical intercept here corresponds to an unpumped gain medium, and is therefore equal to the inverse of the spontaneous emission lifetime $1/\tau$ as before. For the Er^{3+}-doped fiber, τ was measured to be (9.72 $\pm$ 0.11) ms from the linear fit, matching literature data for many types of Er^{3+}-doped silica fiber [53]. This measurement verifies our effective lifetime model and its pump power dependence, and demonstrates how it can be used to measure the spontaneous emission lifetime for new gain media. We can also determine the pump absorption cross-section from the slope in in Fig. 3(c) using (3). After converting from the plotted pump power (P_p) to the pump rate using $\phi_p = P_p/(Ah\nu_p)$, we can use the slope to estimate that $\sigma_{\text{pa}} = (2.24 \pm 0.04) \times 10^{-25}$ m^2 at the pump wavelength of 976 nm, where we calculated the circular mode area A using a 9 μm mode diameter. This estimation again matches with previously reported data from various Er^{3+}-doped silica fibers [54].

Next, we study an 8 cm long Tm^{3+}-doped silica fiber with an absorption of 0.24 dB/cm at 793 nm. Corresponding to Tm^{3+} emission and absorption spectra, we used 1900 nm and 785 nm signal and pump laser diodes, with powers of 90 μW and 1 mW respectively. As before, at each pump power, we fit transfer functions using the measured magnitude and phase responses [Fig. 3(d) and (e)], and represent the inverse of the effective lifetimes with a linear fit [Fig. 3(f)]. It is known that the spontaneous emission lifetime in typical Tm^{3+}-doped silica fibers ($\sim$500 μs) is significantly shorter than that in Er^{3+}-doped silica ($\sim$10 ms). Therefore, shorter lifetimes corresponding to higher energy levels can more significantly alter the phase response around $1/(2\pi\tau_{\text{eff}})$ for Tm^{3+}. This explains why the phase response differs slightly from the transfer function fits at frequencies above 1 kHz in Fig. 3(e). Consequently, two-pole filter fits were used to capture any shorter lifetimes that may be influencing system response at these higher frequencies. However, we did not use the second pole to identify or measure any upper-state lifetimes, as this second-pole may represent the

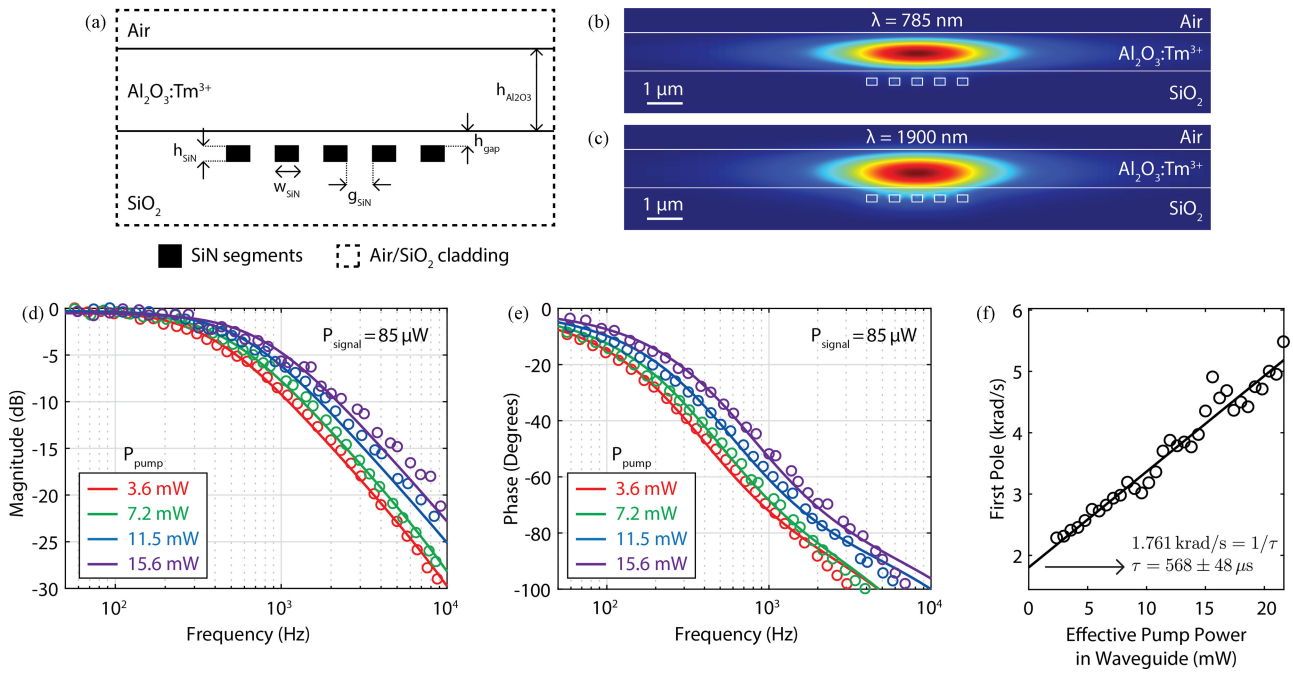

Fig. 4. (a) Inverted ridge waveguide design with blanket-deposited $\mathrm{Al_2O_3{:}Tm^{3+}}$ layer. Fundamental transverse-electric (b) pump and (c) signal mode intensity profiles in the inverted ridge waveguide. (d) Magnitude and (e) phase responses for the $\mathrm{Al_2O_3{:}Tm^{3+}}$ waveguide. (f) Linear fit to the first pole locations calculated from the transfer function fits.

combined result of several energy states with fast dynamics. For the $\mathrm{Tm^{3+}}$-doped fiber, due to the shorter lifetime, we used higher pump powers than in case of $\mathrm{Er^{3+}}$ in order to resolve the differences in the four plotted magnitude and phase responses in Fig. 3(d) and (e). Nevertheless, the linear fit to the first pole locations in Fig. 3(f) indicates a spontaneous emission lifetime of (611 ± 42) μs, agreeing with previous results [55]. Similarly, the pump absorption cross-section at 785 nm is estimated from the slope of the linear fit as $\sigma_{\mathrm{pa}} = (5.60 \pm 0.76) \times 10^{-25}$ m^2, in agreement with previous measurements in $\mathrm{Tm^{3+}}$-doped silica fiber [56].

Lastly, we characterize our newly developed $\mathrm{Al_2O_3{:}Tm^{3+}}$ gain medium. We use the inverted ridge waveguide design in Fig. 4(a) consisting of a $\mathrm{h_{SiN}} = 200$ nm thick multi-segment SiN structure and a $\mathrm{h_{Al2O3}} = 1.1$ μm thick back-end deposited gain medium. The SiN layer was fabricated in a 300 mm CMOS foundry via plasma enhanced chemical vapor deposition and patterned using deep reactive ion etching. Each SiN segment was designed to be $\mathrm{w_{SiN}} = 300$ nm wide, and separated from the adjacent segment by a gap of $\mathrm{g_{SiN}} = 350$ nm. The $\mathrm{Al_2O_3{:}Tm^{3+}}$ gain medium was reactively sputtered on top of the 2 cm long waveguide from Al and Tm targets as a back-end process, using methods outlined previously in [57]. The $\mathrm{Tm^{3+}}$ dopant concentration was $1.6 \times 10^{20}\,\mathrm{cm^{-3}}$, as measured by Rutherford back-scattering.

This specific waveguide design confines majority of pump and signal fundamental transverse-electric (TE) modes in the blanket-deposited gain medium as indicated by the mode intensity profiles in Fig. 4(b) and (c). The pump mode area is calculated from the intensity profile, and is equal to $A = 7.4$ μm^2. The intensity overlap of the pump and signal modes in the gain medium is calculated to be 0.934 by the definition in (4). Corresponding magnitude and phase responses and transfer function fits are plotted in Fig. 4(d) and (e). Due to the smaller mode area and higher pump rate ϕ_p, the transfer functions were measured with pump powers of only up to 20 mW, compared to the 150 mW in case of the $\mathrm{Tm^{3+}}$-doped fiber. We again used two pole filter fits and plotted the corresponding first pole locations in Fig 4(f). Note that the horizontal axis indicating the pump power in the waveguide as well as the powers indicated in the legends have been scaled by the intensity overlap factor Γ. The linear fit yields the spontaneous emission lifetime of (568 ± 48) μs, and an absorption cross-section estimate of $\sigma_{\mathrm{pa}} = (5.83 \pm 0.40) \times 10^{-25}$ m^2. This absorption-cross section shows good agreement with previously reported results for other sputtered $\mathrm{Al_2O_3{:}Tm^{3+}}$ waveguides [58]. The reduction in the measured upper lasing-state lifetime compared to the $\mathrm{Tm^{3+}}$-doped fiber can be explained by the higher $\mathrm{Tm^{3+}}$ dopant concentration in the waveguide.

The frequency domain techniques described here are based on the linear rate equation in (1) and the assumption of small pump modulation depth. Consequently, the mathematical description neglects processes such as energy transfer upconversion or pair-induced quenching. However, such higher-order phenomena are significant for fibers or waveguides with high doping concentrations due to the nonlinear terms they introduce in the rate equations. Especially under strong pumping, as the upper lasing state reaches appreciable population density, additional decay mechanisms become significant with the pathways introduced by energy transfer processes between rare-earth ions. The increased decay rate is observed as a reduction in the effective lifetime at high concentrations and high pump powers [21], [59].

This nonlinear dependence could explain the deviation of the first pole locations plotted in Figs. 3(f) and 4(f) from the linear fit at high pump powers. Moreover, as lightly doped Er-fibers typically have lifetimes over 10 ms [60], [61], the measured value of (9.72 ± 0.11) ms may also indicate the presence of nonlinear energy transfer processes not treated by the presented model.

V. Conclusion

We have identified and detailed a family of frequency domain methods to characterize the system response in optically-pumped rare-earth doped gain media. The methods outlined are based on describing the effective system lifetime as a linear function of the pump rate, and characterizing how this lifetime dictates system bandwidth. We used a two-level model to describe the energy levels in the gain medium, and derived a low-pass filter response between the modulated pump and the resulting population levels that determine the signal gain and absorption. We verified our methods by confirming the well-known spontaneous emission lifetimes and pump absorption cross-sections in Er^{3+} and Tm^{3+}-doped silica fibers. Then we characterized our newly developed Al_2O_3:Tm^{3+} waveguides and measured the spontaneous emission lifetime and 785 nm absorption cross-section as (568 ± 48) μs and $(5.83 \pm 0.40) \times 10^{-25}$ m^2 respectively.

The methods studied in this paper can be expanded by modeling the gain media as systems consisting of more than two energy levels. This is described in detail in the appendix. Obtaining an analytical description with more transitions can yield more accurate system representations and allow spectroscopic measurements of more complex kinetics such as upper state transition or relaxation cross-sections and lifetimes. The pump power dependence of system bandwidth can also be utilized in other media such as semiconductors for excited state lifetime measurements.

Appendix
Frequency Domain Analysis of the Three-Level Gain Medium

The analysis in the text assumes a two-level system consisting of a ground state and an upper lasing state of the rare-earth dopants. We can generalize the frequency domain treatment with an amplitude-modulated pump by including higher energy levels that may be significant in case of short wavelength pump excitations. In general, we can describe the vector of population levels (N) with a set of coupled rate equations that can be written as

$$\frac{d}{dt}N = (Q_0 + Q_m)\,N + P \tag{11}$$

where Q_0, Q_m and P include coefficients and terms involving absorption and emission cross-sections as well as lifetimes of the respective energy levels. Here, we separated the time-dependent part of the right hand side in (11) by defining Q_m to represent the modulated part of the input pump power. Consequently, Q_0 and P are time-independent. Conservation of total number of dopants is implicitly included within the constant term P. This is also why the size of matrix equation (11) is one less than the number of energy levels.

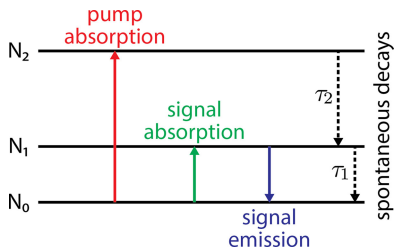

Fig. 5. Energy levels and transitions in a three-level gain medium.

As before, we can represent each population level by a steady state population and a time-varying component due to the amplitude-modulated pump by letting $N = N_{(\mathrm{ss})} + \Delta N$. The steady state solution is obtained under no pump modulation $(Q_m = 0)$, and by setting the time-derivative to zero:

$$N_{(\mathrm{ss})} = -Q_0^{-1} P. \tag{12}$$

We can then rewrite (11) in terms of $N_{(\mathrm{ss})}$ and ΔN, and use the fact that $dN_{(\mathrm{ss})}/dt = 0$. This yields a new set of differential equations that describe the rates of change of ΔN:

$$\begin{aligned}\frac{d}{dt}\Delta N &= (Q_0 + Q_m)(N_{(\mathrm{ss})} + \Delta N) + P \\ &\approx Q_0 \Delta N + Q_m N_{(\mathrm{ss})}.\end{aligned} \tag{13}$$

Here, by using only small modulations of the pump power, we made sure that the population levels only slightly deviate from their steady state values, and $\Delta N + N_{(\mathrm{ss})} \approx N_{(\mathrm{ss})}$. The frequency response is obtained from in (13) by evaluating the Laplace transform of both sides, yielding

$$\Delta N(s) = (sI - Q_0)^{-1} Q_m(s) N_{(\mathrm{ss})}. \tag{14}$$

Once we have the general solution above, we can utilize it in a particular three-level system. A diagram of the energy levels for a typical three-level system is shown in Fig. 5. The total population of dopant ions is given by $N_t = N_0 + N_1 + N_2$. Lifetimes τ_1 and τ_2 correspond to the spontaneous decay rates for transitions between levels $1 \to 0$ and $2 \to 1$ respectively. Specifically, population levels in this three-level system are governed by the rate equations

$$\begin{aligned}\frac{dN_0}{dt} = &-\sigma_{\mathrm{pa}}\phi_p\,(1 + m(t))\,N_0 - \sigma_{\mathrm{sa}}\phi_s N_0 \\ &+ \sigma_{\mathrm{se}}\phi_s N_1 + \frac{N_1}{\tau_1}\end{aligned} \tag{15}$$

$$\frac{dN_1}{dt} = \sigma_{\mathrm{sa}}\phi_s N_0 - \sigma_{se}\phi_s N_1 - \frac{N_1}{\tau_1} + \frac{N_2}{\tau_2}. \tag{16}$$

To match the general form in (11), we rewrite the rate equations as

$$\frac{d}{dt}\begin{bmatrix} N_0 \\ N_1 \end{bmatrix} = \left(\begin{bmatrix} q_{00} & q_{01} \\ q_{10} & q_{11} \end{bmatrix} + Q_m\right)\begin{bmatrix} N_0 \\ N_1 \end{bmatrix} + \begin{bmatrix} p_0 \\ p_1 \end{bmatrix} \tag{17}$$

where the specific coefficients are given by

$$q_{00} = -\sigma_{\mathrm{pa}}\phi_p - \sigma_{\mathrm{sa}}\phi_s \tag{18}$$

$$q_{01} = \sigma_{\mathrm{se}}\phi_s + 1/\tau_1 \tag{19}$$

$$q_{10} = \sigma_{\mathrm{sa}}\phi_s - 1/\tau_2 \tag{20}$$

$$q_{11} = -\sigma_{\mathrm{se}}\phi_s - 1/\tau_1 - 1/\tau_2 \tag{21}$$

$$p_0 = 0 \tag{22}$$

$$p_1 = N_t/\tau_2 \tag{23}$$

$$Q_m = \begin{bmatrix} -\sigma_{\mathrm{pa}}\phi_p m(t) & 0 \\ 0 & 0 \end{bmatrix}. \tag{24}$$

Then, the transfer functions in (14) for the changes in the two population levels ΔN_0 and ΔN_1 can be evaluated as

$$\begin{bmatrix} \Delta N_0(s) \\ \Delta N_1(s) \end{bmatrix} = \frac{-\sigma_{\mathrm{pa}}\phi_p N_{0(\mathrm{ss})} M(s)}{D(s)} \begin{bmatrix} s - q_{11} \\ q_{10} \end{bmatrix} \tag{25}$$

where $M(s)$ is the Laplace transform of the pump modulation $m(t)$, and $D(s) = (s - q_{00})(s - q_{11}) - q_{01}q_{10}$.

As we did for the two-level system, we then relate the change in the population levels to the measured change in the signal output by

$$\begin{aligned} P_{\mathrm{out}} &= P_{\mathrm{in}} \exp\left(-\sigma_{\mathrm{sa}} N_0 L + \sigma_{\mathrm{se}} N_1 L\right) \\ &= P_{\mathrm{out(ss)}} \exp\left(-\sigma_{\mathrm{sa}} \Delta N_0 L\right) \exp\left(\sigma_{\mathrm{se}} \Delta N_1 L\right) \end{aligned} \tag{26}$$

where we defined the steady state signal output power as $P_{\mathrm{out(ss)}} = P_{\mathrm{in}} \exp\left(-\sigma_{\mathrm{sa}} N_{0(\mathrm{ss})} L\right) \exp\left(\sigma_{\mathrm{se}} N_{1(\mathrm{ss})} L\right)$. Since $\Delta N_0 \ll N_{0(\mathrm{ss})}$ and $\Delta N_1 \ll N_{1(\mathrm{ss})}$, we can use a first order Taylor approximation in (26) to approximate the change in the output power and its Laplace transform by

$$\Delta P_{\mathrm{out}}(s) = P_{\mathrm{out(ss)}}(-\sigma_{\mathrm{sa}} \Delta N_0(s) + \sigma_{\mathrm{se}} \Delta N_1(s)) L \tag{27}$$

Finally, we replace $\Delta N_0(s)$ and $\Delta N_1(s)$ in (27) by the solutions in (25) to obtain the full transfer function between the pump modulation $M(s)$ and the change in the measured pump power $P_{\mathrm{out}}(s)$:

$$\begin{aligned} H(s) = &\frac{\sigma_{\mathrm{pa}}\sigma_{\mathrm{sa}}\phi_p N_{0(\mathrm{ss})} P_{\mathrm{out(ss)}} L}{D(s)} \\ &\times \left[s - \left(q_{11} + \frac{\sigma_{\mathrm{se}}}{\sigma_{\mathrm{sa}}} q_{10} \right) \right] \end{aligned} \tag{28}$$

In general, the number of poles in this transfer function is the degree of the polynomial $D(s)$, and is also equal to the size of the matrix equation (11). Specifically, $H(s)$ in (28) has two poles at $s_\pm$ where $D(s_\pm) = 0$. $H(s)$ also has a zero at $s_0 = q_{11} + (\sigma_{\mathrm{se}}/\sigma_{\mathrm{sa}})q_{10} = -1/\tau_1 - (1 + (\sigma_{\mathrm{se}}/\sigma_{\mathrm{sa}}))/\tau_2$. One can confirm the response in (28) converges to that of a two-level system by evaluating the zero and pole locations at the limit where τ_2 approaches 0. In fact, as $\tau_2 \to 0$, it can be shown that $s_0 \to -\infty$, $s_- \to -\infty$, and $s_+ \to -\left((\sigma_{\mathrm{sa}} + \sigma_{\mathrm{se}})\phi_s + \sigma_{\mathrm{pa}}\phi_p + 1/\tau_1\right)$, exactly matching the response in (10) and the $-1/\tau_{\mathrm{eff}}$ pole in (3).

ACKNOWLEDGMENT

The authors would like to thank DARPA DODOS project program managers, Dr. R. Lutwak and Dr. G. Keeler for helpful discussions. N. Li acknowledges a fellowship from the Agency of Science, Technology and Research (A*STAR), Singapore.

REFERENCES

[1] C. R. Giles and E. Desurvire, "Modeling erbium-doped fiber amplifiers," *J. Lightw. Technol.*, vol. 9, no. 2, pp. 271–283, Feb. 1991.

[2] C. Barnard, P. Myslinski, J. Chrostowski, and M. Kavehrad, "Analytical model for rare-earth-doped fiber amplifiers and lasers," *IEEE J. Quantum Electron.*, vol. 30, no. 8, pp. 1817–1830, Aug. 1994.

[3] L. Agazzi *et al.*, "Spectroscopy of upper energy levels in an Er^{3+}-doped amorphous oxide," *J. Opt. Soc. Amer. B*, vol. 30, no. 3, pp. 663–677, 2013.

[4] P. Peterka, I. Kasik, A. Dhar, B. Dussardier, and W. Blanc, "Theoretical modeling of fiber laser at 810 nm based on thulium-doped silica fibers with enhanced $^3H_4$ level lifetime," *Opt. Exp.*, vol. 19, no. 3, pp. 2773–2781, 2011.

[5] G. Rustad and K. Stenersen, "Modeling of laser-pumped Tm and Ho lasers accounting for upconversion and ground-state depletion," *IEEE J. Quantum Electron.*, vol. 32, no. 9, pp. 1645–1656, Sep. 1996.

[6] D. L. Sidebottom, M. A. Hruschka, B. Potter, and R. K. Brow, "Increased radiative lifetime of rare earth-doped zinc oxyhalide tellurite glasses," *Appl. Phys. Lett.*, vol. 71, no. 14, pp. 1963–1965, 1997.

[7] R. Meltzer *et al.*, "Effect of the matrix on the radiative lifetimes of rare earth doped nanoparticles embedded in matrices," *J. Lumin.*, vol. 94, pp. 217–220, 2001.

[8] A. Jha *et al.*, "Rare-earth ion doped TeO_2 and GeO_2 glasses as laser materials," *Progress Mater. Sci.*, vol. 57, no. 8, pp. 1426–1491, 2012.

[9] C. C. Baker *et al.*, "Nanoparticle doping for high power fiber lasers at eye-safer wavelengths," *Opt. Exp.*, vol. 25, no. 12, pp. 13903–13915, 2017.

[10] E. Gaviola, "Ein fluorometer. apparat zur messung von fluoreszenzabklingungszeiten," *Zeitschrift für Physik*, vol. 42, no. 11/12, pp. 853–861, 1927.

[11] P. I. Bastiaens and A. Squire, "Fluorescence lifetime imaging microscopy: Spatial resolution of biochemical processes in the cell," *Trends Cell Biol.*, vol. 9, no. 2, pp. 48–52, 1999.

[12] L. Agazzi, "Spectroscopic excitation and quenching processes in rare-earth-ion-doped Al_2O_3 and their impact on amplifier and laser performance," Ph.D. dissertation, Faculty of Elect. Eng., Math. Comput. Sci., Univ. Twente, Enschede, The Netherlands, 2012.

[13] S. S. Brody, "Instrument to measure fluorescence lifetimes in the millimicrosecond region," *Rev. Sci. Instrum.*, vol. 28, no. 12, pp. 1021–1026, 1957.

[14] G. Peterson and P. Bridenbaugh, "Some studies of relaxation processes in Tb^{3+} using pulsed excitation," *J. Opt. Soc. Amer.*, vol. 53, no. 10, pp. 1129–1138, 1963.

[15] Y. Haas and G. Stein, "Pathways of radiative and radiationless transitions in europium (iii) solutions. Role of solvents and anions," *J. Phys. Chem.*, vol. 75, no. 24, pp. 3668–3677, 1971.

[16] C. Parker and C. Hatchard, "The possibilities of phosphorescence measurement in chemical analysis: Tests with a new instrument," *Analyst*, vol. 87, no. 1037, pp. 664–676, 1962.

[17] L. Riseberg, W. Gandrud, and H. W. Moos, "Multiphonon relaxation of near-infrared excited states of $LaCl_3$:Dy^{3+}," *Phys. Rev.*, vol. 159, no. 2, pp. 262–266, 1967.

[18] W. Ryba-Romanowski, S. Golab, G. Dominiak-Dzik, P. Solarz, and T. Lukasiewicz, "Conversion of infrared radiation into red emission in YVO_4: Yb,Ho," *Appl. Phys. Lett.*, vol. 79, no. 19, pp. 3026–3028, 2001.

[19] D.-L. Zhang and E. Pun, "Accurate measurement of 1.5 μm lifetime of Er^{3+} in $LiNbO_3$ crystals and waveguides," *J. Appl. Phys.*, vol. 94, no. 3, pp. 1339–1346, 2003.

[20] D. Hanna *et al.*, "Frequency upconversion in Tm and Yb: Tm-doped silica fibers," *Opt. Commun.*, vol. 78, no. 2, pp. 187–194, 1990.

[21] G. Nykolak *et al.*, "Concentration-dependent $^4I_{13/2}$ lifetimes in Er^{3+}-doped fibers and Er^{3+}-doped planar waveguides," *IEEE Photon. Technol. Lett.*, vol. 5, no. 9, pp. 1014–1016, Sep. 1993.

[22] X. Orignac, D. Barbier, X. Du, and R. Almeida, "Fabrication and characterization of sol-gel planar waveguides doped with rare-earth ions," *Appl. Phys. Lett.*, vol. 69, no. 7, pp. 895–897, 1996.

[23] N. Mais *et al.*, "Er doped nanocrystalline ZnO planar waveguide structures for 1.55 μm amplifier applications," *Appl. Phys. Lett.*, vol. 75, no. 14, pp. 2005–2007, 1999.

[24] X. Orignac *et al.*, "Sol–gel silica/titania-on-silicon Er/Yb-doped waveguides for optical amplification at 1.5 μm," *Opt. Mater.*, vol. 12, no. 1, pp. 1–18, 1999.
[25] Z. Zhang, K. Grattan, and A. Palmer, "Fiber-optic high-temperature sensor based on the fluorescence lifetime of alexandrite," *Rev. Sci. Instrum.*, vol. 63, no. 8, pp. 3869–3873, 1992.
[26] E. Menzel, K. Rieckhoff, and E. Voigt, "Dynamics of the triplet state of phthalocyanine complexes of the platinum metals in zero field," *J. Chem. Phys.*, vol. 58, no. 12, pp. 5726–5734, 1973.
[27] E. Buurman *et al.*, "Fluorescence lifetime imaging using a confocal laser scanning microscope," *Scanning*, vol. 14, no. 3, pp. 155–159, 1992.
[28] W. Capinski *et al.*, "Thermal-conductivity measurements of GaAs/AlAs superlattices using a picosecond optical pump-and-probe technique," *Phys. Rev. B*, vol. 59, no. 12, 1999, Art. no. 8105.
[29] J. Simsarian, L. A. Orozco, G. Sprouse, and W. Zhao, "Lifetime measurements of the 7p levels of atomic francium," *Phys. Rev. A*, vol. 57, no. 4, pp. 2448–2458, 1998.
[30] T. Fan, A. Cordova-Plaza, M. J. Digonnet, R. Byer, and H. J. Shaw, "Nd:MgO:$\mathrm{LiNbO_3}$ spectroscopy and laser devices," *J. Opt. Soc. Amer. B*, vol. 3, no. 1, pp. 140–148, 1986.
[31] L. Ma *et al.*, "Singlet fission in rubrene single crystal: Direct observation by femtosecond pump-probe spectroscopy," *Phys. Chem. Chem. Phys.*, vol. 14, no. 23, pp. 8307–8312, 2012.
[32] R. A. Palmer, C. J. Manning, J. A. Rzepiela, J. M. Widder, and J. L. Chao, "Time-resolved spectroscopy using step-scan fourier transform interferometry," *Appl. Spectrosc.*, vol. 43, no. 2, pp. 193–195, 1989.
[33] H. Sun and H. Frei, "Time-resolved step-scan Fourier transform infrared spectroscopy of triplet excited duroquinone in a zeolite," *J. Phys. Chem. B*, vol. 101, no. 2, pp. 205–209, 1997.
[34] C. Rödig, I. Chizhov, O. Weidlich, and F. Siebert, "Time-resolved step-scan fourier transform infrared spectroscopy reveals differences between early and late m intermediates of bacteriorhodopsin," *Biophys. J.*, vol. 76, no. 5, pp. 2687–2701, 1999.
[35] K. K. Sharman, A. Periasamy, H. Ashworth, and J. Demas, "Error analysis of the rapid lifetime determination method for double-exponential decays and new windowing schemes," *Analytical Chem.*, vol. 71, no. 5, pp. 947–952, 1999.
[36] K. B. Lee *et al.*, "Application of the stretched exponential function to fluorescence lifetime imaging," *Biophys. J.*, vol. 81, no. 3, pp. 1265–1274, 2001.
[37] W. Blanc *et al.*, "Thulium environment in a silica doped optical fibre," *J. Non-Crystalline Solids*, vol. 354, no. 2–9, pp. 435–439, 2008.
[38] B. Dussardier, W. Blanc, and P. Peterka, "Tailoring of the local environment of active ions in rare-earth-and transition-metal-doped optical fibres, and potential applications," in *Proc. Sel. Topics Opt. Fiber Technol.*, 2012, pp. 95–120.
[39] J. R. Lakowicz and I. Gryczynski, "Frequency-domain fluorescence spectroscopy," in *Topics in Fluorescence Spectroscopy*. New York, NY, USA: Springer-Verlag, 2002, pp. 293–335.
[40] J. Demas, "Phase shift measurements of lifetimes," in *Excited State Lifetime Measurements*, 1st ed. New York, NY, USA: Elsevier, 1983, ch. 4, pp. 50–53.
[41] E. Gratton, D. M. Jameson, and R. D. Hall, "Multifrequency phase and modulation fluorometry," *Annu. Rev. Biophy. Bioeng.*, vol. 13, no. 1, pp. 105–124, 1984.
[42] E. Gratton and M. Limkeman, "A continuously variable frequency cross-correlation phase fluorometer with picosecond resolution," *Biophys. J.*, vol. 44, no. 3, pp. 315–324, 1983.
[43] J. R. Alcala, E. Gratton, and F. G. Prendergast, "Resolvability of fluorescence lifetime distributions using phase fluorometry," *Biophys. J.*, vol. 51, no. 4, pp. 587–596, 1987.
[44] J. Alcala, E. Gratton, and F. G. Prendergast, "Interpretation of fluorescence decays in proteins using continuous lifetime distributions," *Biophys. J.*, vol. 51, no. 6, pp. 925–936, 1987.
[45] G. Laczko *et al.*, "A 10-GHz frequency-domain fluorometer," *Rev. Sci. Instrum.*, vol. 61, no. 9, pp. 2331–2337, 1990.
[46] K. Berndt, H. Duerr, and D. Palme, "Picosecond phase fluorometry by mode-locked CW lasers," *Opt. Commun.*, vol. 42, no. 6, pp. 419–422, 1982.
[47] J. R. Lakowicz *et al.*, "Distance distributions in proteins recovered by using frequency-domain fluorometry. applications to troponin I and its complex with troponin C," *Biochemistry*, vol. 27, no. 26, pp. 9149–9160, 1988.
[48] L. Tolosa *et al.*, "Glucose sensor for low-cost lifetime-based sensing using a genetically engineered protein," *Analytical Biochem.*, vol. 267, no. 1, pp. 114–120, 1999.
[49] P. Ghanouni *et al.*, "Functionally different agonists induce distinct conformations in the g protein coupling domain of the β_2 adrenergic receptor," *J. Biol. Chem.*, vol. 276, no. 27, pp. 24 433–24 436, 2001.
[50] N. Boens *et al.*, "Fluorescence lifetime standards for time and frequency domain fluorescence spectroscopy," *Analytical Chem.*, vol. 79, no. 5, pp. 2137–2149, 2007.
[51] N. Li *et al.*, "High-power thulium lasers on a silicon photonics platform," *Opt. Lett.*, vol. 42, no. 6, pp. 1181–1184, 2017.
[52] Z. Su *et al.*, "Ultra-compact and low-threshold thulium microcavity laser monolithically integrated on silicon," *Opt. Lett.*, vol. 41, no. 24, pp. 5708–5711, 2016.
[53] W. J. Miniscalco, "Erbium-doped glasses for fiber amplifiers at 1500 nm," *J. Lightw. Technol.*, vol. 9, no. 2, pp. 234–250, Feb. 1991.
[54] W. L. Barnes, R. I. Laming, E. J. Tarbox, and P. Morkel, "Absorption and emission cross section of $\mathrm{Er^{3+}}$-doped silica fibers," *IEEE J. Quantum Electron.*, vol. 27, no. 4, pp. 1004–1010, Apr. 1991.
[55] S. D. Agger and J. H. Povlsen, "Emission and absorption cross section of thulium doped silica fibers," *Opt. Exp.*, vol. 14, no. 1, pp. 50–57, 2006.
[56] M. J. Digonnet, *Rare-Earth-Doped Fiber Lasers and Amplifiers, Revised and Expanded*. Boca Raton, FL, USA: CRC Press, 2001.
[57] E. S. Magden *et al.*, "Monolithically-integrated distributed feedback laser compatible with CMOS processing," *Opt. Exp.*, vol. 25, no. 15, pp. 18058–18065, 2017.
[58] P. Loiko and M. Pollnau, "Stochastic model of energy-transfer processes among rare-earth ions. example of $\mathrm{Al_2O_3{:}Tm^{3+}}$," *J. Phys. Chem. C*, vol. 120, no. 46, pp. 26 480–26 489, 2016.
[59] B.-C. Hwang *et al.*, "Cooperative upconversion and energy transfer of new high $\mathrm{Er^{3+}}$- and $\mathrm{Yb^{3+}}$ – $\mathrm{Er^{3+}}$-doped phosphate glasses," *J. Opt. Soc. Amer. B*, vol. 17, no. 5, pp. 833–839, 2000.
[60] K. Ko, M. Demokan, and H. Tam, "Transient analysis of erbium-doped fiber amplifiers," *IEEE Photon. Technol. Lett.*, vol. 6, no. 12, pp. 1436–1438, Dec. 1994.
[61] Z. Zhang, K. Grattan, A. Palmer, B. Meggitt, and T. Sun, "Fluorescence decay-time characteristics of erbium-doped optical fiber at elevated temperatures," *Rev. Sci. Instrum.*, vol. 68, no. 7, pp. 2764–2766, 1997.

Emir Salih Magden received the B.S. degree in electrical engineering from Tufts University *(summa cum laude)*, Medford, MA, USA, in 2012, and the S.M. and Ph.D. degrees in electrical engineering and computer science from Massachusetts Institute of Technology, Cambridge, MA, USA, in 2014 and 2018, respectively. He is currently an Assistant Professor with the Department of Electrical Engineering, Koç University, Istanbul, Turkey, and the Founding Director of Photonic Architectures Laboratory. During his graduate studies, he was involved in the development and optimization of integrated photonic devices and systems for broadband optical signal generation, stabilization, and manipulation as a part of Photonic Microsystems Group, Research Laboratory of Electronics. His current research interests include CMOS-compatible amplifiers and lasers, adaptive integrated photonics, and ultra-broadband on-chip optical networks for communications and sensing applications. He is a three-time recipient of SPIE scholarship in optics and photonics, Amos Eberson Dolbear Scholarship, and a member of Optical Society of America, Tau Beta Pi, and Eta Kappa Nu.

Patrick Callahan received the B.A. degree in physics from Cornell University, New York, NY, USA, in 2008, and the M.Sc. degree in electrical engineering from Johns Hopkins University, Baltimore, MD, USA, in 2010. He is currently working toward the Ph.D. degree in electrical engineering at the Massachusetts Institute of Technology, Cambridge, MA, USA, with interests in low-phase-noise photonic oscillators, photonic analog-to-digital converters, timing-distribution systems, and microwave photonics. He was a part of the EO/IR Systems and Technologies Group, the Johns Hopkins University Applied Physics Laboratory, Laurel, MD, USA, from 2008 to 2011.

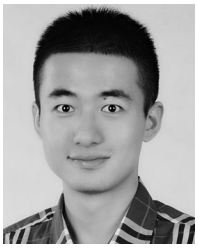

Nanxi Li received the B.E. degree (first class honor) in electrical and electronic engineering from Nanyang Technological University (NTU), Singapore, in 2012, the M.S. degree in applied physics from Harvard University, Cambridge, MA, USA, in 2015, and became a Ph.D. candidate in 2016. Upon his graduation from NTU, he joined Singapore Institute of Manufacturing Technology under Agency for Science, Technology and Research (A*STAR) as a Research Engineer. Concurrently, he is a visiting student with Massachusetts Institute of Technology, Cambridge, MA, USA. His research interests include integrated laser, fiber laser, thin film deposition, and ultrafast optics. He served as a main committee member for the IEEE Photonics Society Singapore Student Chapter from 2012 to 2013, and International Conference on Information Photonics & Optical Communications held in Singapore in 2011. In 2013, he was the recipient of the National Science Scholarship from A*STAR.

Jonathan D. B. Bradley received the B.Eng. and M.A.Sc. degrees in engineering physics from McMaster University, Hamilton, ON, Canada, in 2003 and 2005, respectively, and the Ph.D. degree in electrical engineering from the University of Twente, Enschede, The Netherlands, in 2009. He is an Assistant Professor with the Department of Engineering Physics, McMaster University, Hamilton, ON, USA. In addition to Postdoctoral and Research Scientist appointments at Harvard University (2010–2012) and the Massachusetts Institute of Technology (2012–2013, 2014–2015), he taught undergraduate physics and photonics as an Assistant Professor with the Wilfrid Laurier University, Waterloo, ON, Canada (2013–2014). His research interests include integrated optics, on-chip amplifiers and lasers, microresonator devices, nonlinear nanophotonics, and silicon photonic microsystems. He has authored or coauthored more than 100 journal and conference papers in the field of photonics.

Neetesh Singh received the M.S. degree from The University of New South Wales, Sydney, NSW, Australia, in 2011, and the Ph.D. degree from the University of Sydney, Sydney, NSW, Australia, in 2015. His is currently a Postdoctoral Associate with the Research Laboratory of Electronics, Massachusetts Institute of Technology, Cambridge, MA, USA. His research interests include nonlinear photonics, frequency combs, second and high harmonic generation, and supercontinuum generation in integrated photonics.

Alfonso Ruocco received the Ph.D. degree from Ghent University, Ghent, Belgium, in 2016. During his Masters and Ph.D., he worked with IMEC on semiconductor device simulation with focus on Interdigitated Back Contact (IBC) solar cells, and advanced infrared spectrometers on a silicon chip. Previously, he was a Postdoctoral Associate with the Research Laboratory of Electronics, Massachusetts Institute of Technology, Cambridge, MA, USA. He is currently a Research Associate with the Cambridge Graphene Centre, and the Department of Engineering, Cambridge University, Cambridge, U.K. His research interests include integrated optoelectronics and silicon photonic device architectures.

Leslie A. Kolodziejski is currently a Principal Investigator with the Research Laboratory of Electronics, Massachusetts Institute of Technology (MIT), Cambridge, MA, USA. She joined the Electrical and Computer Engineering Department, Purdue University, in 1986, as an Assistant Professor. In 1988, she joined the Department of Electrical Engineering and Computer Science, MIT. Her research interests include the gaseous source epitaxy of II–VI and III–V compound semiconductors with applications in the overgrowth of InGaAsP onto patterned surfaces for DFB lasers and WDM filters for all-optical networks, the fabrication photonic bandgap devices and structures, and the growth and fabrication of novel high-power lasers. She was the recipient of the Presidential Young Investigator Award from the National Science Foundation and Young Investigator Award from the Office of Naval Research, both in 1987 and was honored with the Karl van Tassel Career Development Chair from 1992 to 1993 and with the Esther and Harold E. Edgerton Career Development Chair from 1993 to 1996.

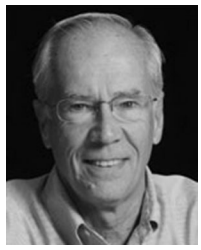

Erich P. Ippen received the S.B. degree in electrical engineering from the Massachusetts Institute of Technology, Cambridge, MA, USA, in 1962, and the M.S. and Ph.D. degrees from the University of California, Berkeley, CA, USA, both in electrical engineering, in 1965 and 1968, respectively. He is a Principal Investigator with the Research Laboratory of Electronics, Massachusetts Institute of Technology. He holds appointments as the Elihu Thomson Professor of Electrical Engineering Emeritus and Professor of Physics Emeritus. He was a member of the technical staff at Bell Laboratories from 1968 to 1980 where he was one of the founders of the field of femtosecond optics. He joined the MIT faculty in 1980. His research interests include femtosecond science and ultra-highspeed devices, techniques to exploit the time resolution femtosecond pulses provide, and probing ultrafast phenomena in materials. He is a member of both the National Academy of Sciences and the National Academy of Engineering, and is also a fellow of the American Academy of Arts and Sciences.

Michael R. Watts received the Bachelor of Science degree in electrical engineering from Tufts University, Middlesex County, MA, USA, in 1996 and the S.M. and Ph.D. degrees from the Massachusetts Institute of Technology (MIT), Cambridge, MA, USA, in 2001 and 2005, respectively. After graduation, he joined the Draper Laboratory as a Member of Technical Staff in their Fiber Optics Group. In 1999, he became a Draper Fellow. In 2005, he joined Sandia National Labs where he led their silicon photonics effort as a Principal Member of Technical Staff. In 2010, he returned to MIT as an Associate Professor. He is currently a Principal Investigator with the Research Laboratory of Electronics, and a member of the Department of Electrical Engineering and Computer Science, MIT. His research interests include photonic microsystems for low-power communications, sensing, and microwave-photonics applications.